# Visualizations of critical point topology in the skin-friction field of near-wall turbulence

**Christoph Brücker**[1]
[1]Institute of Mechanics and Fluiddynamics, TU Bergakademie Freiberg, Germany
christoph.bruecker@gmx.net

**Abstract** The recent discovery of rare backflow events in turbulent boundary layer flows based on the analysis of DNS data (Lanears et al. 2012) has raised again the unmet need of accurate near-wall measurements to detect such events. It has further been shown that there is a strong correlation between the appearance of critical points (zero WSS) and their relation to large-scale events in the log-layer. Only recently, such data were gained from highly resolved DNS data which allowed to analyze the topology around these critical points (Cardesa et al. 2014). Up to now there is no experimental prove of the topological pattern and the behavior of such critical points. As discussed in Lanears et al. (2012), the discovered rare events have been so far not been detected using state-of-the art techniques to measure the velocity close to the wall such as hot-wire or LDA probes. This is because the sensing volume needs to be located away from the wall, and the frequency of occurrence drastically reduces with distance from the wall. Second, in order to capture the strong velocity gradients within the viscous sublayer, the diameter of the measurement volumes has to be as small as the viscous length scale, which brings along a drastic reduction of the sampling rate. Only when the DNS data revealed such events, the careful re-arrangement of the experimental studies allowed to indirectly detect such events using points-wise measurements. The present paper shows results of 2D micropillar array wall-shear measurements according the method described in Brücker et al. (2005) where the micropillars were tailored to detect events with low magnitude of WSS in an otherwise turbulent flow. The results clearly indicate the rare events of backflow and the structure of the topology is seen immediately from the raw visualization pictures taken from the micropillar array recordings.

**Keywords:** micropillar, imaging, skin-friction, critical points, turbulence, rare backflow

## 1 Introduction

The near-wall flow topology in turbulent wall-bounded flows is one of the topics that is still of high interest to understand the complex mutual interaction of events in the log-layer with the near-wall region. The careful analysis of DNS data of turbulent channel flow by Lanears et al. [1] has shown that there are rare events in the near-wall region, where backflow occurs. These seem to occur with a percentage of less than 0.2% within the flow which makes it difficult to capture such events in experimental studies. This might be the reason why some speculation about the existence of near-wall backflow has grown in the past. Only when the DNS data revealed such events, the careful revision of the experimental studies of the authors allowed to indirectly detect such events using points-wise measurements. As soon as backflow is present, it is reasonable to expect that critical points CP (zero WSS) are seen, although not necessarily all regions with negative streamwise WSS need to be CPs. Detailed data was gained recently from highly resolved DNS that allowed to analyze the topology around these CPs in the WSS field (Cardesa et al. [2]). The results show a strong correlation between the appearance of CPs and their relation to large-scale events in the log-layer. The overall picture is that a CP marks the tail end of a large-scale structure and it is formed when a vortex at the tail end of the large-scale structure is transported toward the wall. Their extreme nature leads to a long-lasting effect in form of low-streamwise-velocity regions in their “wake” that extend over 800 wall units downstream of a CP. Up till now, however, there is no experimental prove for the existence of such CPs at the wall and nothing is known about their topological patterns.

## 2 Methods

Herein, results are shown for micropillar recordings in an oil flow tunnel installed at Erlangen University. The flow tunnel was designed for high-resolution optical measurements of transitional and turbulent

boundary-layer flow along a flat plate at zero-pressure-gradient (ZPG). The temperature of the working fluid (Odina oil, density $\rho$ = 840 kg $m^{-3}$) and therefore its viscosity could be varied to cover a broader range of Reynolds-numbers in the flow. In this experiment it was set to room temperature with a kinematic viscosity $\nu = 11\times10^{-6}$ $m^2/s$. A thin flat plate (total length of 3 meters) with a sharp trailing edge was placed in the middle of the test section. Different configurations of micropillar arrays distributed over the plate were used at various flow conditions for testing of the sensing capabilities described in Brücker et al. [3]. Our studies were focused on a region located 1.9m downstream of the leading edge. At a free stream velocity $U_0$ = 4.2 m/s the Reynolds-number based on the streamwise position of the micropillars is $Re = 7\times10^5$, thus the boundary layer is in an early turbulent state. The Reynolds-number $Re_\tau$ defined in terms of the friction velocity $u_\tau$ = 0.22 m/s and the flow thickness $\delta$ amounts to $Re_\tau = u_\tau\ \delta\ /\nu \approx 940$. The viscous length scale $l_v = \vartheta/u_\tau$ is 50µm and the non-dimensional viscous time-scale is $t^+ = t\ u_\tau^2/v$. Throughout the paper, the coordinate directions are streamwise (x), spanwise (y) and wall-normal (z) directions. A port with a 2D array of 30×30 flexible filaments on its surface was placed at the predefined location inside the plate such that the port surface was flush with the plate's upper surface. The filaments (diameter $D+\approx0.8$, height $L+\approx10$, material: Poly-Dimethylsiloxane, $\rho$ =1050 kg/$m^3$, Young's modulus in the liquid environment $E\approx1.23\times10^6$ N/$m^2$) extend from the port surface in wall-normal direction into the flow and have a regular spacing of $10x^+$ and 10 $y^+$. Recordings were taken with a high-speed camera (Photron APX-RS, 1024×1024 px, 1500fps) with a temporal resolution of 2,93 $t^+$. Within the viewing field of the camera a number of 9×9 pillars can be seen. Typically a total number of 6000 frames were stored on a disc corresponding to a time-span of about 17.500 $t^+$.

## 3 Results

In the selected experiments, the micropillar structures were tailored towards higher flexibility such that they bend more easily with the flow than in the previous experiments with structures that bend in the order of the pillar diameter (Brücker [4], Große & Schröder [5]). More flexible sensors have a higher sensitivity as shown in Brücker et al. [6], which is of importance if one is interested in resolving low magnitudes of WSS values in an otherwise turbulent flow where the absolute WSS values can range from zero (CP in the WSS field) to typically three-times the mean, sometimes even five-times the mean, see Örlü & Schlatter [7]. Therefore high resolution power is especially required near CPs where WSS is zero. Figure 1 illustrates the bending of the filaments (also called "reconfiguration", compare Vogel [8]) in a shear flow apparatus built for calibration purpose. In the linear-elastic regime (the limit is $\Delta s/L \cong 25\%$, this has also been shown by Paek & Kim [9]) the flexible micropillar shows a 10-times higher sensitivity compared to a less flexible micropillar that is designed to capture the whole span of expected WSS values (dotted line over a span of 0 – 3 times the mean $\tau_W$). Because of the higher flexibility the structure bends down with the flow, for mean flow conditions the tip is already down to a level $z+ \approx 6.6$, see case D in figure 1. Hence, although at first one might disqualify such 10+ long filaments as WSS sensors following the design rules given in Brücker et al. [6], they can still remain fully submerged within the viscous sublayer due to their reconfiguration with the flow. On the other hand, as seen in figure 1 the higher flexibility comes with the disadvantage of increased non-linear behavior at higher WSS when bending of the structures is >= 0.5*L*. There, the filaments are out of the linear-elastic regime and they increasingly become sensitive to wall-normal velocity fluctuations, too. These regions of large WSS values are not in focus here and the presented recordings do not claim to represent reliable measurements at such levels, see the discussion at the end.

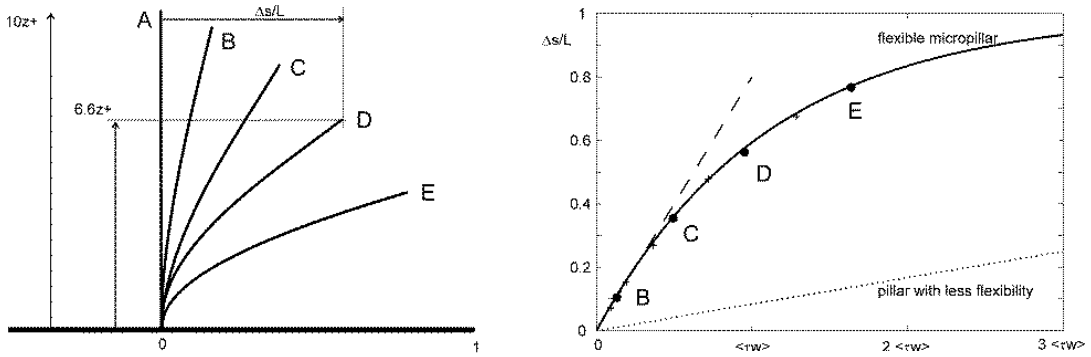


Fig 1: Reconfiguration of the tailored micropillars in a calibration shear flow [10]. Symbols: tip displacement measurements corresponding to the reconfiguration, solid line: curve fit with $\Delta s/L=1-\exp(0.018*\tau)$. A roughly 10-times higher sensitivity (dashed line approximating the linear-elastic range) is achieved at low WSS values compared to a less flexible structure designed for measuring the complete range of WSS in the flow (dotted line representing the linear-elastic behavior over a range 0 – 3 times the mean $\tau_W$).

The response of the micropillars is represented by a 2nd order mechanical system of a damped oscillator as derived in Brücker et al. [6]. The first natural frequency of the filaments in air is 1.2kHz which was measured in an oscillating flow driven by counter-facing anti-phasic loud-speakers. In the oil bath damping is higher and the system is overdamped as the quality factor Q=0.14 is less than 1/sqrt(2), see eq. (13) in Brücker et al. [6]. In such an overdamped case the characteristic time-scale is the response time and no resonance exists at all. This response time is the ratio of effective damping to effective spring stiffness as given in eq. (8) in Brücker et al. [6] and is calculated for the present case to be approx. $8.8\ t^+$. This is expected to be sufficiently high to resolve the relevant WSS fluctuations near the CPs. Based on the DNS results of Cardesa et al. [2] the formation of CP's is linked to large scale events in the buffer layer, thus the involved frequencies are expected to be lower than the peak frequencies related to the smallest scales in the turbulent flow.

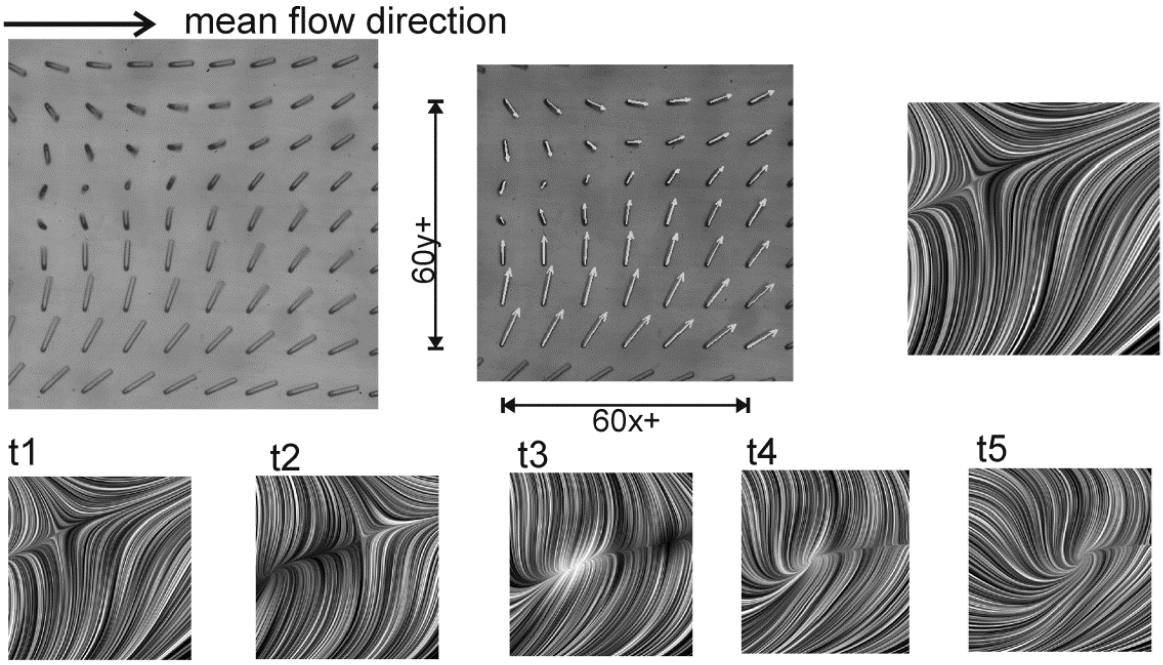


Fig 2: Evolution of a saddle- node pair [10]. Flow is from left to right. Top row, left: original raw image, middle: vectorization of the inner part (7×7 vectors), right: LIC picture generated from the vectorization with cubic interpolation. Bottom row: evolution of topology over 5 successive pictures ($\Delta t^+ = 2.93$).

The micropillar bending is given by the evolution of the end-to-end vector in between the base fixation of the filament and the tip position in the extended situation. Measurements with the camera looking from the above onto the wall surface provide only the projection of the end-to-end vector in the wall-parallel x-y-plane $\boldsymbol{Q}$ with its components *Qx* and *Qy*. This describes the WSS vector in orientation and magnitude. Following the discussion in Cardesa et al. [2] the local topology of CPs in WSS is given by the similarity invariant of the no-slip tensor *A* computed at the CP. Within a linear approximation in the vicinity of the CP (compare eq. (5) in [2]) the invariant simplifies to

$$p = tr(A) = \mathrm{tr}\left(\begin{bmatrix} \partial^2 u/\partial x \partial z & \partial^2 u/\partial y \partial z \\ \partial^2 v/\partial x \partial z & \partial^2 v/\partial y \partial z \end{bmatrix}\right) \approx \mathrm{tr}\left(\begin{bmatrix} \partial Q_x/\partial x & \partial Q_x/\partial y \\ \partial Q_y/\partial x & \partial Q_y/\partial y \end{bmatrix}\right) = div(\boldsymbol{Q})$$

Therefore CPs can be found in our results where the divergence $p = \nabla \cdot \boldsymbol{Q}$, calculated from the Q-vector field on the regular grid by central difference schemes, is large. This criterion was used herein for conditional sampling of the data to exclude phases of low turbulent action from the further analysis as the flow at Re ≈ $7\times10^5$ is not in a fully developed turbulent state. Therefore, all time-steps were chosen where the average p-value in the field was larger than $2.5p_{rms}$. This left roughly 10% of the total number of images (n=641) with a high divergence. A typical picture of the flow at a peak value of $p/p_{rms} = 5$ is given in Fig. 2. Note that the raw image is of high contrast and the filaments are easy to see by the naked eye. A saddle point has appeared on the left side of the image with backflow on its left branch. This structure is transported with a streamwise convection velocity of $U_c^+ \approx 8.5$. In the wake of the saddle, an unstable node is seen in the third image of the sequence. This supports the observation of Cardesa et al. [2] that CPs always occur in saddle-node pairs with a certain lifetime. In our results their connection shows a strong converging flow pattern in spanwise direction and the node is somewhat lagging the motion of the saddle. Both exist for a time-span of at least $t^+=8.8$. In the last image of the sequence, the node seems to transform into a focus. Negative streamwise WSS is now a result of strong curvature of the flow around the CP as seen by the LIC illustration. This strong tilt of the WSS vectors against the mean-flow direction leads us to conclude that the underlying structures in the buffer layers are large ones, however in no case bypass rollers that might still exist in the flow as reminders of the transition process. Otherwise, a stronger coherence in spanwise direction should be present, which isn't seen.

From all conditional sampled data the JPDF of streamwise and spanwise component of ***Q*** was plotted in fig. 3. The vectors are normalized with the length *L*. Note that the JPDF in the higher WSS-regions is much skewed towards the mean as expected from the non-linear behavior shown in figure 1. These regions however are not within the focus herein. To highlight the nature of possible backflow events all vectors where the streamwise bending component is $Q_x/L<0.15$ were plotted as dots. The results indicate that the events with negative streamwise WSS are not only distributed in regions of low WSS but also stem from regions where the spanwise component is of considerable magnitude. Thus, events with strong spanwise WSS seem to correlate with such negative streamwise backflow as a consequence of strong curvature of fluid motion in the wall-parallel plane.

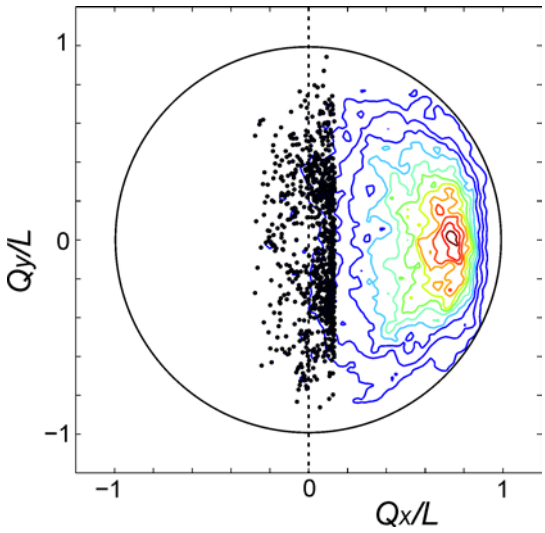


Fig 3: Contours of 2D distribution of probability density of micropillar configuration vector ***Q*** components in the x-y-plane in the turbulent boundary layer [10]. Mean streamwise component is $Q_x/L\approx0.6$. The dots indicate all vectors with the streamwise component *Qx/L* less than 0.15. Contour lines are calculated from counting the number of vectors in boxes of the size 0.02×0.02. The contour levels are equally spaced in 11 steps.

This conclusion is supported by the angular distribution of ***Q*** shown in Fig. 4. Regions with streamwise backflow components are found more often in the arc from ± 90° - 115° than at angles larger than ± 115°. Note that such vectors appear in less than 0.1% of the number of the conditional samples. The accumulated number of vectors with an orientation larger than ± 90° in the complete sequence is about 0.05%, thus these events are extremely rare as found in the DNS data, too.

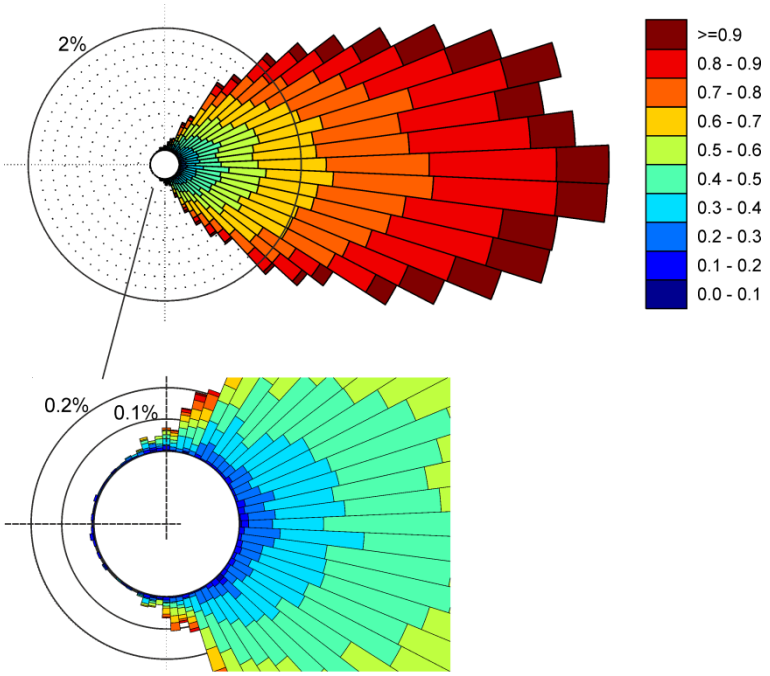


Fig 4: Probability distribution of the orientation of ***Q*** in the x-y-plane [10]. Flow is from left to right. The bottom figure shows an enlarged image of the data given above. Angular steps are in 5°. The color indicates the magnitude $|Q|/L$ in the ranges given in the legend bar.

## 4 Discussion and Conclusions

The direct imaging of the WSS topology near CPs using micropillar imaging in near-wall turbulence shows striking similarities with the recent high-resolution details gained from DNS data reported in [2], although the experiments were run at lower Reynolds-numbers at $Re_\tau \approx 940$. The extreme rarity of the backflow events observed in DNS of channel flows reported in [1] has been proven to hold also in turbulent boundary layer flows at ZPG as shown herein. Those backflow events occur in our experiments at about 0.05% of the recorded images and are always linked to CPs. There is a preference of these backflow regions with WSS vectors that are strongly tilted against the streamwise direction in angles between 90°-115°.

A necessary condition for the detection of such events with sufficient spatial resolution in the array of sensors was tailoring the sensitivity of the pillars to low WSS values in an otherwise turbulent flow, where the WSS magnitude spans a wide range. Thus, the structures were made more flexible at the expense of losing accuracy at WSS values in the higher range. Therefore the recorded patterns are of rather qualitative nature, one may understand those as visualizations analogue to the Schlieren visualizations in compressible flows. On the other hand, detecting the topological pattern near a CP requires sufficient resolution power of the sensors against the measurement uncertainty which cannot be achieved in arrays with sensors tuned to capture the full range of WSS levels. Therefore such events of weak near-wall backflow may have been overlooked so far, which is where we see the benefit of the tailored structures. The evidence is provided herein for a certain phenomenon that was looked for and where the sensors were tailored for, while for other applications or phenomena the significant uncertainty associated with larger bending may disqualify a physical interpretation. A possible practical solution for the resolution problem could be to simultaneously use structures of different effective stiffness next to each other to cover different dynamic ranges with comparable accuracy. However it is difficult to prevent flow disturbance and mutual interaction if a number of sensors with different sensitivities are placed close to each other. Another possible solution is the use of channeling optics as proposed by the author in another communication, which allows focusing simultaneously on a large number of individual sensors with high resolution in each channel.

Finally, the hitherto agreed upon limit for the length of micropillar sensors for quantitative WSS measurements, i.e. the classical 5z+ definition for the thickness of the viscous sublayer, possibly needs some revision in the context described herein. This definition of the viscous sublayer is linked to the local mean, still measurements may focus on WSS levels far away from the mean, an example thereof given herein for the lower range near CP's in the WSS field. The existing DNS data from Cardesa et al. [2] may help to analyze in the region around a CP how far away from the wall (<= 10z+) the linear approximation of the no-slip tensor still is valid, possibly beyond the classical 5z+ definition. Therefore, DNS coupled with simulations on the load profile on such filaments in the WSS field may give a definite answer about the measurement precision in such conditions.

**Acknowledgement**
This material is based upon work supported by the Air Force Office of Scientific Research, Air Force Material Command, USAF under Award No. FA9550-14-1-0315 and program manager Gregg Abate. The measurements in the Erlangen oil channel were made possible by the support of the DFG and the LSTM which is gratefully acknowledged here.

## 5 References

[1] Lenaers P, Li Q, Brethouwer G, Schlatter P, Örlü R (2012) Rare backflow and extreme wall-normal velocity fluctuations in near-wall turbulence. *Phys. Fluids* 24, 035110.

[2] Cardesa J, Monty J, Soria J, Chong M (2014) Skin-friction critical points in wall-bounded flows. 1st Multiflow Summer Workshop, IOP Publishing, Journal of Physics: Conference Series 506, 01200.

[3] Brücker C, Spatz J, Schröder W (2005) Feasibility of wall shear stress imaging using micro structured surfaces with flexible micropillars. *Exp. Fluid* 39, 2005, 464-474.

[4] Brücker C (2008) Signature of varicose wave packets in the viscous sublayer. *Phys. Fluids* 20, 061701.

[5] Grosse S, Schröder W (2009) Wall-shear stress patterns of coherent structures in turbulent duct flow. *J. Fluid Mech.* 633, 147-158.

[6] Brücker C, Bauer D, Chaves H (2007) Dynamic response of micro-pillar sensors measuring fluctuating wall-shear-stress. *Exp. Fluid* 42, 737-749.

[7] Örlü R, Schlatter P (2011) On the fluctuating wall-shear stress in zero-pressure-gradient turbulent boundary layers. *Phys. Fluids* 23, 021704.

[8] Vogel S (1989) Drag and reconfiguration of broad leaves in high winds. *J. Exp. Bot* 40, 941-948.

[9] Paek J, Kim J (2014) Microsphere-assisted fabrication of high aspect-ratio elastomeric micropillars and waveguide, *Nature Communications* 5, 3324.

[10] Brücker C (2015) Evidence of rare backflow and critical points in skin-friction fields using micropillar imaging. Phys Fluids 27, 031705; doi: http://dx.doi.org/10.1063/1.4916768